Modeling kinetics of diffusion-controlled surface wrinkles

Yong Ni,* Linghui He, and Qihan Liu

CAS Key Laboratory of Mechanical Behavior and Design of Materials, and Department of Modern Mechanics, University of Science and Technology of China, Hefei, Anhui 230026, People's Republic of China

(Received 12 June 2011; revised manuscript received 28 July 2011; published 15 November 2011)

Nonlinear wrinkling of a compressed film on a soft substrate in the presence of inhomogeneous swelling actuation strain caused by solvent diffusion is studied. The simulation relies on a continuum model which integrates phase field microelasticity and Föppl–von Kármán plate theory. We show that the wrinkling morphologies developed in the diffusive domain exceeding a critical compression are confined and become shape and size dependent. A rich variety of wrinkling patterns observed in experiments including hexagonal ordered, dimple, or peanut structures, are numerically recovered, depending on the distribution of diffusion-mediated actuation strain. A cascade feature of the diffusion-coupled wrinkle is demonstrated as well: There are two ranges of solvent concentration within which the sequences of wrinkling pattern are different.

DOI: 10.1103/PhysRevE.84.051604 PACS number(s): 68.08.−p, 62.20.mq, 68.55.−a, 64.75.Yz

I. INTRODUCTION

A compressive thin film (sheet or layer) on soft substrates may release stress by developing surface wrinkles through Euler-type buckling instability [1–3]. The wrinkling morphology is determined by the balance between the decreasing stretch energy of the film and the increasing energies due to film bending and substrate distortion. To form ordered wrinkling patterns, various strategies have been explored to regulate distribution of in-plane compression in the film, including a prepatterned substrate [4], an elastomeric mold [5], a cracked film [6], capillarity [7], and thermally, mechanically, or osmotically induced compression [8–12]. Application of such surface wrinkles has been found not only in measuring the elastic modulus of thin films [13] and understanding their hierarchical morphogenesis [14–16], but also in guiding three-dimensional microfabrications of smart adhesion devices [17,18], microlens arrays [19], self-assembled gears [20], flexible electronics [21], etc. Recent experiments demonstrate that the wrinkling instability can be mediated by mass diffusion which produces a spatiotemporal swelling actuation strain (eigenstrain). The nonuniformity of the eigenstrain may lead to more interesting controllable wrinkling morphologies such as hexagonal ordered, and dimple or peanut structures [22–26], which are all beyond the previously observed straight wrinkles, labyrinths, herringbone, and chessboardlike patterns in the absence of diffusion. Exploring the phenomena and the underlying dynamics is obviously of important significance for developing versatile approaches to generate hierarchical [27] or multicomponent [28] polymer patterns.

Wrinkling of thin films in the absence of mass diffusion has been extensively studied previously, where the compressive stress before buckling onset is usually assumed to be uniform. Under uniaxial compression, a film may buckle with straight wrinkles, and the critical strain, equilibrium wavelength, and amplitude can be predicted by a set of simple scaling laws [29–31]. Similar results based on energy minimization are obtainable for the cases of herringbone and checkerboard wrinkling patterns [32–34]. The cubic anisotropic elasticity of the film is found to alter the orientation of the wrinkle and decrease the values of the equilibrium wavelength and amplitude [35,36]. In addition, finite-deformation analysis of buckling indicates that the wavelength is strain dependent rather than constant in the small-deformation theory [37]. A series of nonlinear analyses utilizing the relaxation method [38–44], the finite-element method [45–47], and the iteration method [48] are developed to investigate other problems. These involve wrinkle growth and coarsening on viscous substrates [38–42], orientational ordering of wrinkles [44], and postwrinkling patterns under different boundary conditions [45–48].

In contrast, little is known about wrinkling of thin films coupled with diffusion. In this case the compressive stress before buckling is in general not uniform because the diffusion-induced swelling is heterogeneous. Wrinkles may appear only in diffusive domains with compressive stress exceeding certain critical values, and thus are confined due to diffusion. Since the process of diffusion usually is much slower than that of wrinkling, the development of wrinkles depends on when and where the compressive stress exceeds the buckling threshold. This paper studies nonlinear evolution of diffusion-coupled wrinkles. The main goal is to explore the effect of diffusion-mediated actuation strain on the formation and transition mechanisms of such wrinkling patterns as hexagonal ordered, dimple, or peanut structures. To this end, we propose a continuum model integrating phase field microelasticity (PFM) [49] and the Föppl–von Kármán plate theory [50] to track the temporal evolution of a film-substrate system driven by an arbitrarily distributed diffusion-mediated swelling actuation strain. Our numerical simulations show how and why the interplay between diffusion and buckling can lead to a rich variety of wrinkling patterns.

II. MODELING

As shown in Fig. 1, we consider an elastic thin film of thickness h on a soft elastic substrate. It is assumed that a certain solvent may be adsorbed and may diffuse in the film, causing the film to swell. Such an effect of solvent adsorption can be characterized by a hydrostatic actuation strain (swelling strain). In general, the distribution of the actuation strain is both position and time dependent, inducing inhomogeneous

*yni@ustc.edu.cn

 ©2011 American Physical Society

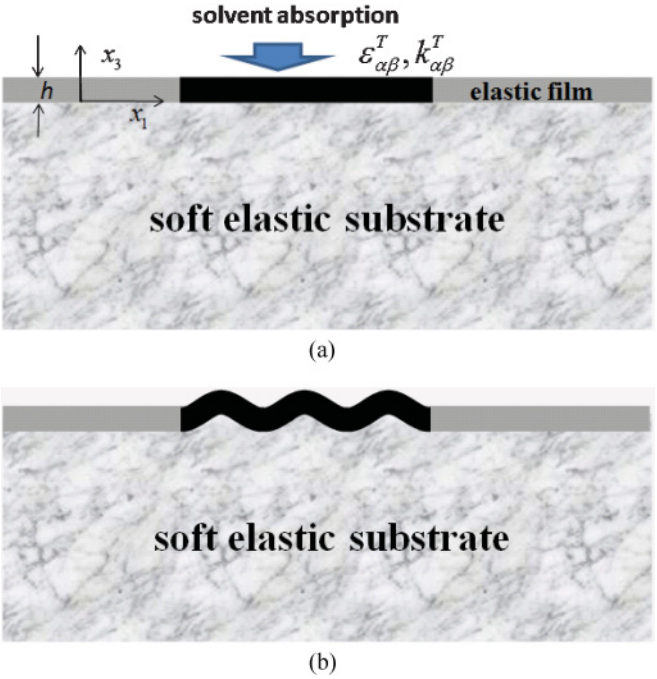

FIG. 1. (Color online) A sketch of a surface wrinkle in a film-substrate system with inhomogeneous actuation strain (in-plane expansion $\varepsilon^T_{\alpha\beta}$ and eigencurvature $k^T_{\alpha\beta}$) induced by solvent absorption: (a) a flat configuration, (b) a locally wrinkled configuration.

stress in the film. Therefore, when the compressive stress somewhere in the film exceeds the critical value, wrinkles appear there due to elastic buckling. The goal of this section is to formulate a dynamic model for the diffusion-mediated wrinkling phenomenon. For convenience, a coordinate system is introduced as in Fig. 1, and the usual summation convention is adopted for repeated indices, with greek and latin indices running from 1 to 2 and 1 to 3, respectively. A comma stands for differentiation with respect to the suffix index.

We model the film as an isotropic von Kármán plate and the substrate as an elastically isotropic half space. At any time t, the actuation strain at a point $\mathbf{x}$ in the film is denoted by $\varepsilon^*_{\alpha\beta}(\mathbf{x},t)$. Since the film is very thin, one can expand $\varepsilon^*_{\alpha\beta}(\mathbf{x},t)$ with respect to the thickness coordinate up to the first order, i.e., $\varepsilon^*_{\alpha\beta}(\mathbf{x},t) = \varepsilon^T_{\alpha\beta}(x_1,x_2,t) + x_3 k^T_{\alpha\beta}(x_1,x_2,t)$. Clearly, $\varepsilon^T_{\alpha\beta}(x_1,x_2,t)$ is the in-plane eigenstrain in the midplane $x_3 = 0$, and $k^T_{\alpha\beta}(x_1,x_2,t)$, possessing the dimension of reversed length, is interpreted as the eigencurvature induced by solvent adsorption. We assume that both $\varepsilon^T_{\alpha\beta}(x_1,x_2,t)$ and $k^T_{\alpha\beta}(x_1,x_2,t)$ are proportional to the solvent concentration $c(x_1,x_2,t)$ in the midplane, and thus express $\varepsilon^*_{\alpha\beta}(\mathbf{x},t)$ by

$$\varepsilon^*_{\alpha\beta}(\mathbf{x},t) = \left(\varepsilon_0 + \varepsilon_0' \frac{x_3}{h}\right) c(x_1,x_2,t)\delta_{\alpha\beta}, \tag{1}$$

where ε_0 and ε_0' are two constants related to the hydrostatic actuation strain, and $\delta_{\alpha\beta}$ is the Kronecker delta which equals 1 for $\alpha = \beta$ and vanishes for $\alpha \neq \beta$. The total strain in the film is the sum of the elastic strain $\bar{e}_{\alpha\beta}$ and the actuation strain $\varepsilon^*_{\alpha\beta}$, i.e.,

$$\bar{\varepsilon}_{\alpha\beta} = \bar{e}_{\alpha\beta} + \varepsilon^*_{\alpha\beta}. \tag{2}$$

According to the Kirchhoff hypothesis, the displacement components at any point in the thin film $\bar{u}_i$ ($i = 1$–3) can be written as

$$\begin{aligned} \bar{u}_\alpha &= u_\alpha - x_3 w_{,\alpha}, \\ \bar{u}_3 &= w(x_1,x_2). \end{aligned} \tag{3}$$

in which u_α and w are, respectively, the in-plane and out-of-plane displacement components of the midplane. The total strain in the Föppl–von Kármán sense reads

$$\bar{\varepsilon}_{\alpha\beta} = \tfrac{1}{2}(\bar{u}_{\alpha,\beta} + \bar{u}_{\beta,\alpha}) + \tfrac{1}{2}\bar{u}_{3,\alpha}\bar{u}_{3,\beta}. \tag{4}$$

The substitution of Eqs. (1)–(3) into (4) gives the elastic strain

$$\begin{aligned} \bar{e}_{\alpha\beta} = {} & \frac{1}{2}(u_{\alpha,\beta} + u_{\beta,\alpha}) + \frac{1}{2} w_{,\alpha} w_{,\beta} - x_3 w_{,\alpha\beta} \\ & - \left(\varepsilon_0 + \varepsilon_0' \frac{x_3}{h}\right)\delta_{\alpha\beta} c(x_1,x_2,t). \end{aligned} \tag{5}$$

We now consider the energy of the system. The energy of the film consists of the concentration-dependent chemical free energy and the strain energy, and can be represented by

$$\begin{aligned} F^{\text{film}} = \int_{-h/2}^{h/2}\int_{-\infty}^{\infty}\int_{-\infty}^{\infty} \Big[& f(c) + \beta_c(\nabla c)^2 \\ & + \frac{1}{2}\bar{\sigma}_{\alpha\beta}\bar{e}_{\alpha\beta}\Big] dx_1\, dx_2\, dx_3. \end{aligned} \tag{6}$$

In the integrant of the above equation, the first term $f(c)$ is the chemical energy density. Treating the film with solvent absorption as a binary solid solution and using the regular solution approximation, we have

$$f(c) = \Lambda k_B T\{\Omega c(1-c) + [c\ln c + (1-c)\ln(1-c)]\}, \tag{7}$$

in which Ω is a dimensionless parameter characterizing the atom exchange interaction energy in terms of $\Lambda k_B T$, Λ denotes the number of atoms per unit volume, k_B is Boltzmann's constant, and T stands for the absolute environment temperature. The second term, $\beta_c(\nabla c)^2$, is the gradient chemical energy due to the nonuniform concentration, with β_c being the gradient coefficient. The third term is the elastic energy density, where the stress $\bar{\sigma}_{\alpha\beta}$ relates to the elastic strain by the Hooke law

$$\bar{\sigma}_{\alpha\beta} = \frac{2\mu_f}{1-\upsilon_f}[(1-\upsilon_f)\bar{e}_{\alpha\beta} + \upsilon_f \bar{e}_{\gamma\gamma}\delta_{\alpha\beta}], \tag{8}$$

with μ_f and υ_f being, respectively, the shear modulus and Poisson ratio of the film. With the aid of Eqs. (5) and (8), Eq. (6) becomes

$$F^{\text{film}} = h\int_{-\infty}^{\infty}\int_{-\infty}^{\infty}[f(c) + \beta_c(\nabla c)^2]dx_1 dx_2 + E_s^{\text{film}} + E_b^{\text{film}}, \tag{9}$$

in which E_s^{film} is the stretching energy given by

$$\begin{aligned} E_s^{\text{film}} = \frac{\mu_f h}{1-\upsilon_f}\int_{-\infty}^{\infty}\int_{-\infty}^{\infty} \Big[& e_{11}^2 + e_{22}^2 + 2\upsilon_f e_{11} e_{22} \\ & + 2(1-\upsilon_f)e_{12}^2\Big] dx_1\, dx_2, \end{aligned} \tag{10}$$

with

$$e_{\alpha\beta} = \tfrac{1}{2}(u_{\alpha,\beta} + u_{\beta,\alpha}) + \tfrac{1}{2} w_{,\alpha} w_{,\beta} - \varepsilon_0 c\delta_{\alpha\beta}, \tag{11}$$

and E_b^{film} is the bending energy expressed by

$$E_b^{\text{film}} = \frac{\mu_f h^3}{12(1-\upsilon_f)} \int_{-\infty}^{\infty}\int_{-\infty}^{\infty} \left\{ \left(\Delta w + \frac{2\varepsilon_0' c}{h} \right)^2 - 2(1-\upsilon_f) \left[\left(w_{,11} + \frac{\varepsilon_0' c}{h} \right) \left(w_{,22} + \frac{\varepsilon_0' c}{h} \right) - (w_{,12})^2 \right] \right\} dx_1\, dx_2. \tag{12}$$

The elastic energy of the substrate can be written by using the Gauss divergence theorem as

$$F^{\text{sub}} = \frac{1}{2} \int_{-\infty}^{\infty}\int_{-\infty}^{\infty} T_i^s u_i^s \, dx_1\, dx_2, \tag{13}$$

where T_i^s and u_i^s are, respectively, the interfacial traction and displacement components at the film/substrate interface. For simplicity, we assume that the substrate is elastically incompressible, with the Poisson's ratio $\upsilon_s = 0.5$. By invoking the Green's function for a semi-infinite elastic half space, the expression of T_i^s can be obtained as

$$T_i^s = \frac{1}{(2\pi)^2} \int \tilde{M}_{ij} \tilde{u}_j^s e^{i\xi_\alpha x_\alpha} \, d\xi_1\, d\xi_2, \tag{14}$$

where μ_s is the shear modulus, ξ_α is the component of the Fourier vector, $\tilde{M}_{ij}$ is a matrix defined by

$$\tilde{M}_{ij} = \mu_s \xi \begin{bmatrix} 1+n_1^2 & n_1 n_2 & 0 \\ n_1 n_2 & 1+n_2^2 & 0 \\ 0 & 0 & 2 \end{bmatrix}, \tag{15}$$

with

$$\xi = \left(\xi_1^2 + \xi_2^2\right)^{1/2}, \quad n_1 = \xi_1/\xi, \quad n_2 = \xi_2/\xi, \tag{16}$$

and $\tilde{u}_j^s$ denotes the Fourier transform of u_j^s:

$$\tilde{u}_j^s(\boldsymbol{\xi}) = \int_{-\infty}^{\infty}\int_{-\infty}^{\infty} u_j^s(x_1,x_2) e^{-i(\xi_1 x_1 + \xi_2 x_2)} \, dx_1\, dx_2. \tag{17}$$

Obviously, if there is no interfacial debonding during the wrinkling process, the displacement vector is continuous across the film/substrate interface, i.e.,

$$u_i^s = u_i. \tag{18}$$

The total energy of the system has the form

$$F^{\text{tot}} = F^{\text{film}} + F^{\text{sub}}. \tag{19}$$

At mechanical equilibrium, the variation of F^{tot} with respect to u_α and w must vanish. The condition $\delta F^{\text{tot}}/\delta u_\alpha = 0$ gives the in-plane equilibrium equation

$$\sigma_{\alpha\beta,\beta} = T_\alpha^s, \tag{20}$$

where $\sigma_{\alpha\beta}$, defined in the following, is the component of membrane force in the film:

$$\sigma_{\alpha\beta} = \frac{2h\mu_f}{1-\upsilon_f} [(1-\upsilon_f) e_{\alpha\beta} + \upsilon_f e_{\gamma\gamma} \delta_{\alpha\beta}]. \tag{21}$$

By using Eqs. (11), (14), (18), and (21), it is inferred from Eq. (20) through Fourier transformation that

$$\tilde{u}_\alpha = \tilde{C}_{\alpha\beta}^{-1} \tilde{\rho}_\beta, \tag{22}$$

in which

$$\tilde{u}_\alpha(\boldsymbol{\xi}) = \int u_\alpha(x_1,x_2) e^{-i(\xi_1 x_1 + \xi_2 x_2)} \, dx_1\, dx_2, \tag{23}$$

$$\tilde{C}_{\alpha\beta} = \left[\frac{h\mu_f}{1-\upsilon_f}(1-\upsilon_f)\xi^2 + \mu_s \xi \right] \delta_{\alpha\beta} + \left[\frac{h\mu_f}{1-\upsilon_f}(1+\upsilon_f)\xi^2 + \mu_s \xi \right] n_\alpha n_\beta, \tag{24}$$

$$\tilde{\rho}_\beta = \int \sigma_{\beta k,k}^0 e^{-i\xi_\alpha x_\alpha} \, dx_1\, dx_2 - \tilde{M}_{3\beta} \tilde{w}, \tag{25}$$

$$\sigma_{\beta k,k}^0 = \frac{h\mu_f}{1-\upsilon_f} [-2(1+\upsilon_f)\varepsilon_0 c_{,\beta} + (1+\upsilon_f) w_{,\beta k} w_{,k} + (1-\upsilon_f) w_{,kk} w_{,\beta}]. \tag{26}$$

This result, when inserted in Eq. (11), leads to the expression of in-plane elastic strain

$$e_{\alpha\beta}(x_1,x_2) = \langle e_{\alpha\beta} \rangle + \frac{1}{2} \int_{|\underset{\sim}{\xi}| \neq 0} \frac{i(\xi_\alpha \tilde{G}_{\beta k} + \xi_\beta \tilde{G}_{\alpha k}) \tilde{\rho}_k e^{i\xi\cdot\mathbf{r}}}{(2\pi)^2} d^2\xi - \left(\varepsilon_0 c \delta_{\alpha\beta} - \frac{1}{2} w_{,\alpha} w_{,\beta} \right), \tag{27}$$

where $\langle e_{\alpha\beta} \rangle = 0$ for the case of the thin film bonded on a thick substrate, and $\tilde{G}_{\alpha\beta} = \tilde{C}_{\alpha\beta}^{-1}$ is given by

$$\tilde{G}_{\alpha\beta} = \frac{\delta_{\alpha\beta}}{h\mu_f \xi^2 + \mu_s \xi} - \frac{[h\mu_f(1+\upsilon_f)\xi^2 + (1-\upsilon_f)\mu_s \xi] n_\alpha n_\beta}{2(h\mu_f \xi^2 + \mu_s \xi)[h\mu_f \xi^2 + (1-\upsilon_f)\mu_s \xi]}. \tag{28}$$

In the meantime, the condition $\delta F^{\text{tot}}/\delta w = 0$ is reduced to the out-of-plane equilibrium equation of the film

$$D\Delta^2 w + \frac{(1+\upsilon_f) D \varepsilon_0'}{h} \Delta c - (\sigma_{\alpha\beta} w_{,\alpha})_{,\beta} + T_3^s = 0, \tag{29}$$

with $D = \mu_f h^3/[6(1-\upsilon_f)]$ being the bending rigidity.

The coupled integral equations (27) and (29) determine the deformations of the film and substrate at equilibrium, but they are very difficult to be solved directly. For this reason, we replace Eq. (29) by the Ginzburg-Landau kinetic equation

$$\frac{\partial w}{\partial t} = -\Gamma \frac{\delta F^{\text{tot}}}{\delta w}, \tag{30}$$

where Γ is a kinetic coefficient which characterizes the relaxation rate of the wrinkling process in the overdamped dynamics. Apparently, Eq. (30) recovers Eq. (29) in the steady state, and governs the equilibrium solution of the out-of-plane displacement $w(x_1,x_2,t)$. To determine the concentration $c(x_1,x_2,t)$, two diffusion processes with conservative and nonconservative solvent mass must be distinguished. The evolution of $c(x_1,x_2,t)$ is described by

$$\frac{\partial c}{\partial t} = \nabla M \nabla \frac{\delta F^{\text{tot}}}{\delta c} \tag{31}$$

in the former case, while it is described by

$$\frac{\partial c}{\partial t} = -\Gamma_c \frac{\delta F^{\text{tot}}}{\delta c} \tag{32}$$

in the latter case. Here M and Γ_c are the related kinetic coefficients. Once $w(x_1,x_2,t)$ and $c(x_1,x_2,t)$ are obtained, the equilibrium in-plane deformation can be solved numerically from Eq. (27) with the help of the fast Fourier transform technique.

III. SIMULATIONS AND RESULTS

A. Size- and shape-dependent wrinkles

We will presume mass conservation of the solvent and solve the coupled equations (27), (30), and (31) numerically by using a spectral method [51]. These equations are scaled so that all physical lengths are measured in unit l ($r' = r/l$, $l = h$) and the time t in unit τ ($t' = t/\tau$, $\tau = h/\Gamma\mu_s$). The size of the periodic computational domain is set as $512\ l \times 512\ l$. The semi-implicit algorithm is adopted, and the iterative schemes of Eqs. (30) and (31) are written as

$$\tilde{w}^{(n+1)} = \frac{\tilde{w}^{(n)} + \Delta t'\left[A\varepsilon_0'\xi^2\tilde{c}^{(n)} + i\xi_\beta(\sigma_{\alpha\beta}w_{,\alpha}/h\mu_s)_\xi^{(n)}\right]}{1 + \Delta t'(2\xi + D^*\xi^4)}, \tag{33}$$

$$\tilde{c}^{(n+1)} = \frac{\tilde{c}^{(n)} - \Delta t' M^*\xi^2\left[\left(\frac{1}{\mu_s}\frac{\partial f}{\partial c}\right)_\xi^{(n)} - \frac{\tilde{\sigma}_{\alpha\alpha}^{(n)}\varepsilon_0}{h\mu_s} + A\varepsilon_0'(-\xi^2\tilde{w}^{(n)} + 2\varepsilon_0'\tilde{c}^{(n)})\right]}{1 + 2\Delta t'\beta^* M^*\xi^4}, \tag{34}$$

where the notation $(\,)_\xi$ or tilde $\tilde{(\,)}$ stands for the Fourier transform, $\Delta t'$ is the scaled time increment, $D^* = \mu_f/[6(1-v_f)\mu_s]$, $A = (1+v_f)D^*$, $\beta^* = \beta/(\mu_s h^2)$, and $M^* = M/\Gamma$. Throughout the paper, the values of the input parameters are taken as $v_f = 0.3$, $\beta^* = 1$, $\Lambda k_B T/\mu_s = 6$, $\Omega = 2.4$, $\mu_f/\mu_s = 525$, $\Delta t' = 0.2$, and $M^* = 0.01$ (unless otherwise noted). The choice of $M^* \ll 1$ reflects the fact that wrinkling usually takes place much faster than solvent diffusion.

To test our modeling, we consider sinusoidal wrinkling of the film bearing a uniform and constant actuation strain $\varepsilon^*_{\alpha\beta} = \varepsilon_{\text{pre}}\delta_{\alpha\beta}$. The problem has been studied analytically, with the equilibrium wavelength λ_c, critical buckling strain ε_c, and amplitude of out-of-plane displacement δ given by [48]

$$\frac{\lambda_c}{2\pi h} = \left[\frac{\mu_f(1-v_s)}{3\mu_s(1-v_f)}\right]^{1/3}, \quad \varepsilon_c = \frac{1}{4(1+v_f)}\left(\frac{2\pi h}{\lambda_c}\right)^2, \quad \frac{\delta}{h} \cong \left(\frac{\varepsilon_{\text{pre}}}{\varepsilon_c} - 1\right)^{1/2}. \tag{35}$$

Setting $c = 1$, $\varepsilon_0 = \varepsilon_{\text{pre}}$, $\varepsilon_0' = 0$, and $M^* = 0$, we simulate the wrinkling phenomenon based on Eqs. (27) and (30). It is found that $\varepsilon_c = 0.0077$ and $\lambda_c/h = 31.6$, which are very close to the analytical predictions. As plotted in Fig. 2, equilibrium amplitudes of sinusoidal wrinkles at compressive strains larger than ε_c are also obtained numerically and compared with the analytical results. The good agreement manifests the capability of the present model in the simulation of nonlinear wrinkles.

We then turn our attention to the case when the film is under inhomogeneous compression. Assume that a constant swelling strain ε_{pre} is prescribed within a circular domain of radius R in the film. In this situation wrinkling can only initiate in the domain as ε_{pre} exceeds a critical value ε_c', because outside that region the film is under tension. Figure 3 plots the simulated critical strain ε_c' for the confined wrinkling as a function of the reduced domain size $R' = R/\lambda_c$. It is found that, for $R' < 1$, the critical strain ε_c' is significantly higher than that for the sinusoidal wrinkling ε_c. The wrinkling patterns under various domain sizes at $\varepsilon_{\text{pre}} = \varepsilon_0 = 3\varepsilon_c$ are shown in Fig. 4. With the decrease of R', the pattern becomes severely confined, leading to a size-dependent morphology ranging from the labyrinth form, to the checkerboard, to dimple structures. These simulated morphologies are very close to the observation in Ref. [19]. Usually, the shape of the compressive domain can be changed by solvent diffusion. Figure 5 illustrates wrinkling patterns as well as the strain distributions induced by uniform swelling strains given in a square or a rectangular domain in the film. We see that, close to the boundary, the maximum compression always

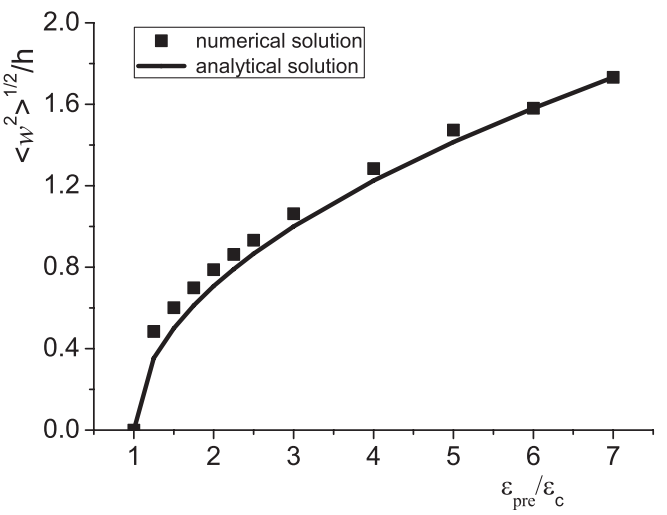

FIG. 2. The amplitudes of an equilibrium sinusoidal wrinkle as a function of the reduced eigenstrain $\varepsilon_{\text{pre}}/\varepsilon_c$ from numerical simulation and analytical solution.

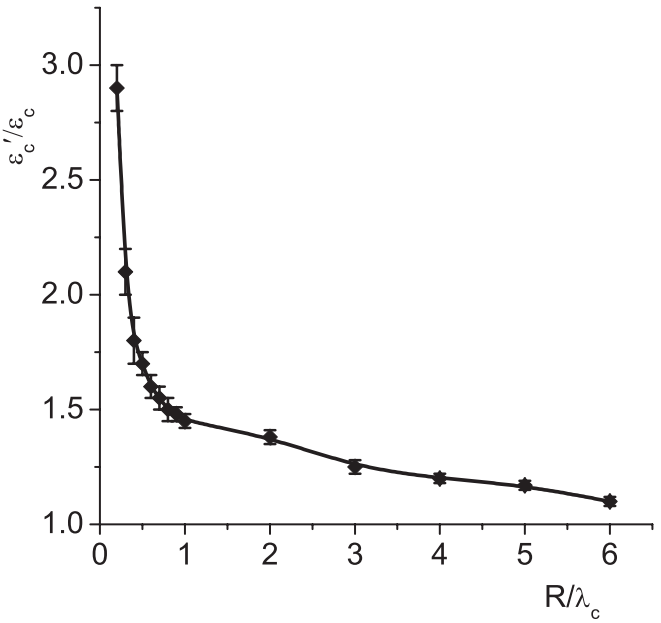

FIG. 3. The critical confined wrinkling strain $\varepsilon_c'/\varepsilon_c$ as a function of the reduced domain size R/λ_c.

appears in the direction parallel to the boundary, and the wrinkles tend to be aligned perpendicularly to the direction of maximum compression. This may provide an explanation for experimental observations that the wrinkles tend to grow perpendicular to the diffusion front [22,27]. In addition, Fig. 5(c) also shows the formation of a stripe wrinkle along the y axis because in most parts of the domain the maximum compression is along the x axis, as marked in the lighter shade in Fig. 5(d). This demonstrates a shape-dependent wrinkle: A large aspect ratio of the diffusion domain promotes a uniaxial compression, and thus is favorable for stripe wrinkle formation.

B. Formation of hexagonal wrinkling pattern

Previous analyses indicate that a chessboardlike wrinkle will be formed when the film undergoes equal-biaxial homogeneous compression slightly above the critical value [47]. When the wrinkling is coupled to diffusion, however, a hexagonal pattern is observed at the value of $\varepsilon_{\text{pre}}/\varepsilon_c$ just above unity [23,25,26]. In our simulation, a checkerboard pattern is recovered, as shown in Fig. 6(a), when the input parameters $c = 0.4$, $\varepsilon_0 = 0.02$, $\varepsilon_{\text{pre}} = \varepsilon_0 c = 0.008$, $\varepsilon_c = 0.0077$, $\varepsilon_0' = 0$, and $M^* = 0$ are chosen so that the film is under homogeneous precompression slightly above the critical value. If, however, diffusion is allowed ($M^* = 0.01$) and $\varepsilon_{\text{pre}}/\varepsilon_c = 0.008/0.0077$ is fixed, then the simulated wrinkling patterns in Figs. 6(b)–6(f) deviate significantly from the checkerboard. Figure 6(b) corresponds to the vanishing eigencurvature (i.e., $\varepsilon_0'/h = 0$) induced by solvent absorption is zero, and no hexagonal pattern is formed in this case. Figures 6(c)–6(f) illustrate wrinkling patterns formed at eigencurvatures ranging from $\varepsilon_0' = 0.001$ to 0.05. It is apparent that increasing positive eigencurvature promotes the formation of hexagonally arrayed islands. A similar wrinkling pattern of hexagonal order has been observed in Refs. [25] and [26]. The concentration profiles corresponding to the diffusion-coupled wrinkles in Figs. 6(a)–6(f) with a miscibility gap ($\Omega > 2$) are plotted in Fig. 7. We see that the wrinkles occur only in the concentration-rich area where the compressive stress exceeds the buckling threshold. The inhomogeneous distributions of concentration and out-of-plane displacement tend to be commensurate with each other to reach a low-energy configuration. In particular, the eigencurvature induced by solvent diffusion is found to play an important role in the formation of hexagonal wrinkle patterns. Figure 8 further demonstrates the result for a film with a negative eigencurvature ($\varepsilon_0' = -0.05$). Very close to the experimental observation [23] which is also shown in Figs. 8(a) and 8(b) reveals that the negative eigencurvature facilitates formation of a hexagonal dimple structure. Previous

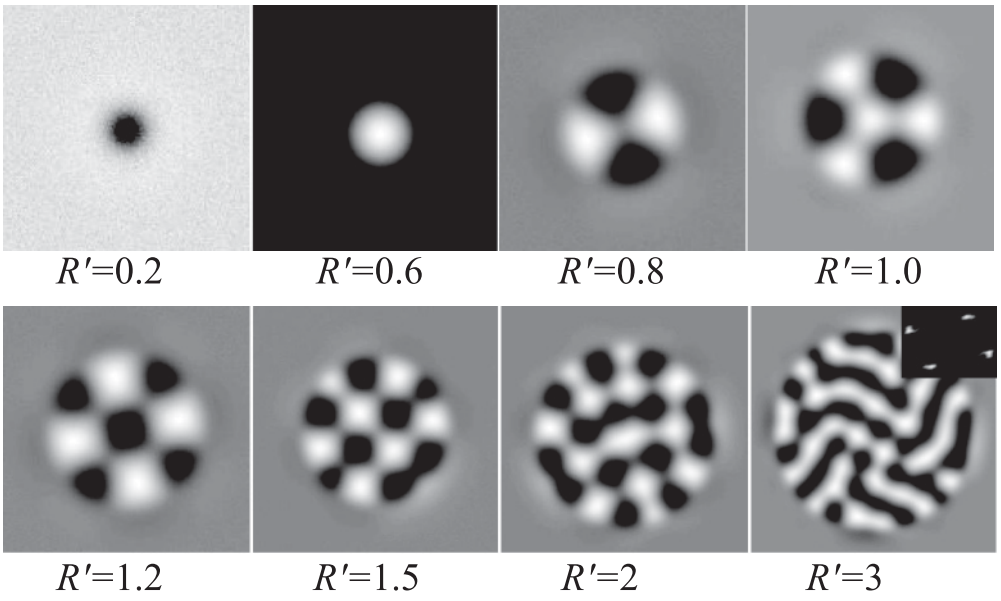

FIG. 4. The simulated wrinkling pattern as a function of the reduced diffusive domain size $R' = R/\lambda_c$ under $\varepsilon_0 = 3\varepsilon_c$, $\varepsilon_0' = 0$, at $t' = 10^4$, with the black to white shading mapping the value of w from negative to positive.

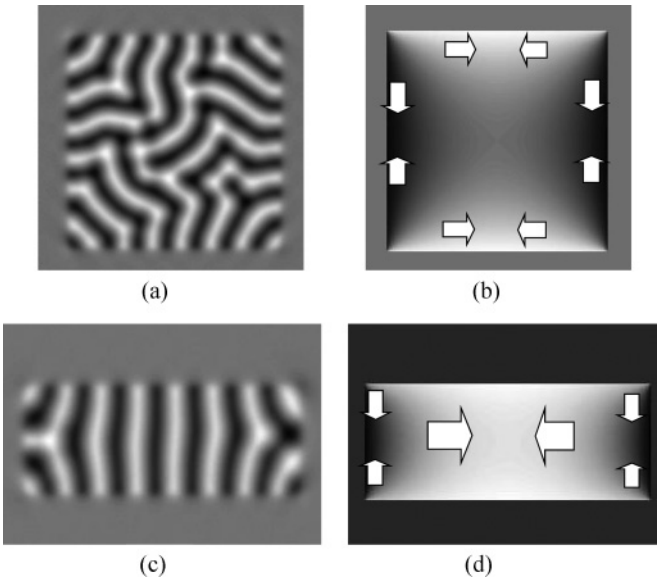

FIG. 5. Simulated shape-dependent wrinkling pattern at $t' = 10^4$ in (a) a square domain $L = 3\lambda_c$ long, (c) a rectangular domain with $L_x = 3\lambda_c$, $L_y = 1.2\lambda_c$. (b), (d) Visualization of the corresponding profile of the reduced $(|\sigma_{xx}| - |\sigma_{yy}|)/\mu_s$ in the domains before the onset of wrinkling, respectively, with the darker to lighter shading mapping its value from negative to positive.

studies indicate that, in the absence of mass diffusion, the wrinkling pattern of the film evolves from a chessboard to a herringbone pattern with increasing equal-biaxial supercritical compression [45]. Nonetheless, recent experiments show that, if the compression is induced by solvent diffusion, the wrinkling pattern appears in the sequence from hexagonal order, to a peanut structure, and finally to a herringbone pattern with the increase of solvent absorption [25,26]. Similar transitions of such wrinkling patterns are confirmed in Fig. 9, where the simulated wrinkles and concentration profiles are visualized under different average solvent concentrations at

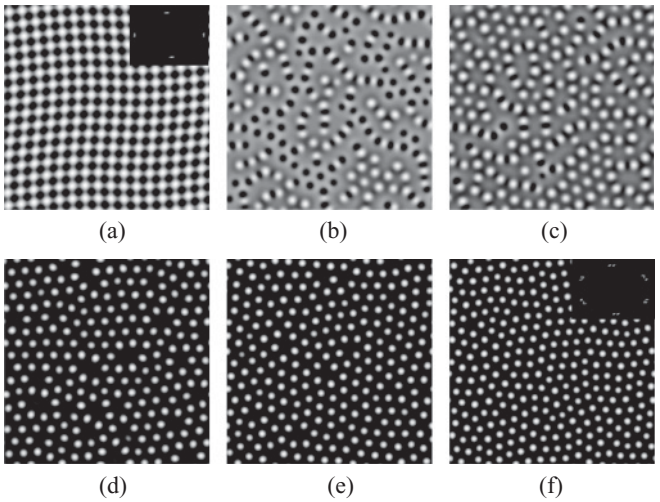

FIG. 6. Simulated wrinkling patterns in the film obtained at $t' = 10^4$ for all cases with $c_0 = 0.4$, $\varepsilon_0 = 0.02$, and with additional parameters (a) $M^* = 0$, $\varepsilon_0' = 0$, (b) $\varepsilon_0' = 0$, (c) $\varepsilon_0' = 0.001$, (d) $\varepsilon_0' = 0.005$, (e) $\varepsilon_0' = 0.01$, (f) $\varepsilon_0' = 0.05$.

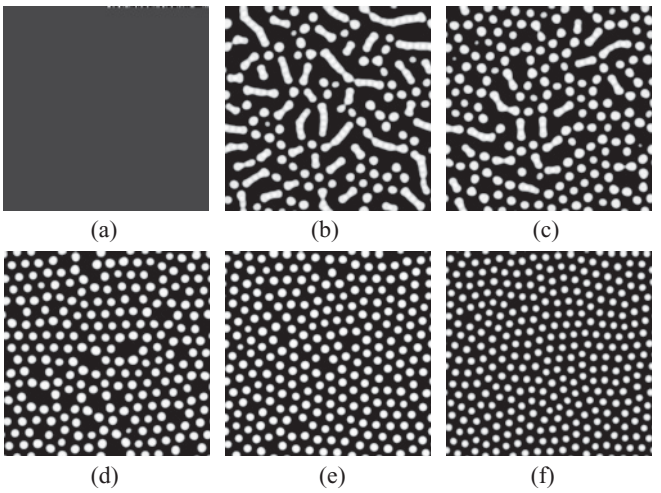

FIG. 7. (a)–(f) are the corresponding simulated concentration profiles of the cases in Figs. 6(a)–6(f), respectively.

$\varepsilon_0 = 0.02$ and $\varepsilon_0' = 0.02$. When the average compression induced by solvent absorption is slightly above the buckling threshold, finite concentration fluctuation driven by diffusion leads to an inhomogeneous wrinkle in the diffusive domain with the compression exceeding a critical value, as shown in Figs. 9(c) and 9(f). If the average compression is significantly higher than the critical value, the diffusion-induced concentration fluctuation becomes less important because the wrinkle can occur almost everywhere. This is why the simulated wrinkling pattern in Fig. 9(a) is very close to a herringbone structure, although there is a finite concentration fluctuation due to diffusion.

C. Cascade evolution of diffusion-controlled wrinkles

Before the onset of buckling, the membrane strain in the film is determined by the solvent concentration. Thus there exists a critical concentration c_{cri} of solvent absorption, above which the membrane strain is larger than the critical buckling strain and the film wrinkles. In other words, whether the film is wrinkled or not can be tracked by probing the concentration-dependent free energy of the film-substrate system. For the sinusoidal wrinkling [48] mentioned before, the total free

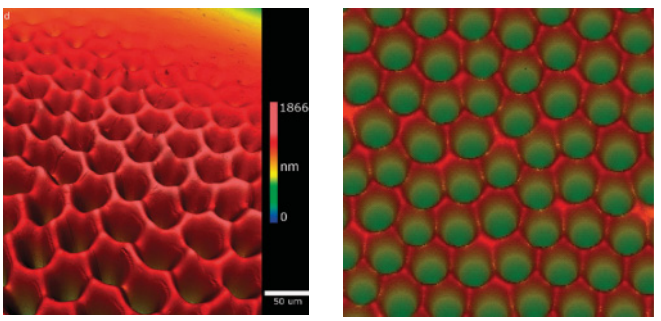

FIG. 8. (Color online) Comparison between the observed wrinkling pattern in Ref. [23] with the simulated dimple pattern under the parameters $c_0 = 0.4$, $\varepsilon_0 = 0.02$, and $\varepsilon_0' = -0.05$ (reproduced with permission).

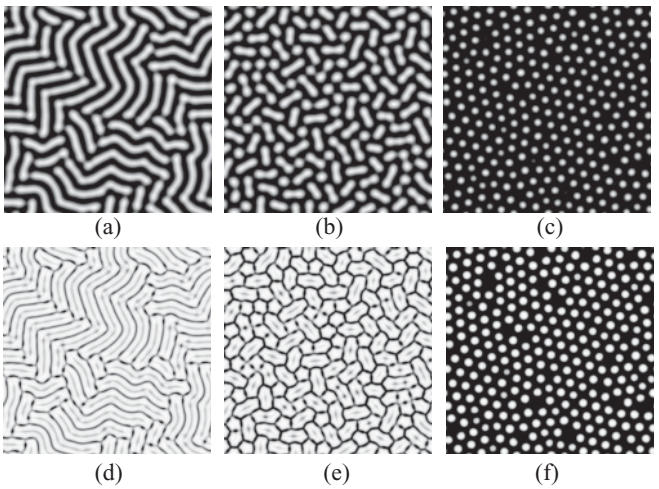

FIG. 9. Simulated patterns of surface wrinkles and concentration profiles in the film with different levels of solvent absorption. The top and bottom rows indicate the profiles of the out-of-plane displacement and the concentration at $t' = 2 \times 10^3$, $\varepsilon_0 = 0.03$, $\varepsilon_0' = 0.02$ under (a) $c = 0.95$, (b) $c = 0.6$, (c) $c = 0.4$, respectively.

energy in Eq. (5) becomes

$$\frac{F^{\text{tot}}}{hS} = \Lambda k_B T\{\Omega c(1-c) + [c\ln c + (1-c)\ln(1-c)]\} + \frac{2\mu_f(1+\upsilon_f)}{(1-\upsilon_f)}\left[\varepsilon_{\text{pre}}^2 - \frac{(1+\upsilon_f)}{2}(\varepsilon_{\text{pre}} - \varepsilon_c)^2 \times H(\varepsilon_{\text{pre}} - \varepsilon_c)\right], \quad (36)$$

where S is the area of the film, $\varepsilon_{\text{pre}} = \varepsilon_0 c$, ε_c is the critical buckling strain defined in Eq. (35), and $H(\varepsilon_{\text{pre}} - \varepsilon_c)$ is the Heaviside function. The flat configuration of the film possesses similar form of total energy as in Eq. (36), except the second term on the right-hand side is replaced by $2\mu_f(1+\upsilon_f)\varepsilon_{\text{pre}}^2/(1-\upsilon_f)$. Figure 10 plots the variations of the total energies for the flat and wrinkled film configurations with solvent concentration. It is found that there are two concentration ranges A and B, separated by a critical concentration c_{cri}. The value of c_{cri} is determined by equating the total energy of the flat configuration to that of the sinusoidally wrinkled one:

$$c_{\text{cri}} = \frac{1}{4(1+\upsilon_f)\varepsilon_0}\left[\frac{3\mu_s(1-\upsilon_f)}{\mu_f(1-\upsilon_s)}\right]^{2/3}. \quad (37)$$

In range A, $c < c_{\text{cri}}$, the free energy of the flat configuration is lower than that of the wrinkled configuration. As a result, the system can reduce the free energy only by diffusion-controlled concentration separation, i.e., phase separation. After the concentration in the solvent-rich area exceeds the critical concentration c_{cri}, local wrinkling can develop. However, in range B, where $c > c_{\text{cri}}$, the film can spontaneously evolve into a wrinkled configuration without concentration changes. This is the first step of system equilibration to reduce the free energy. The second step can start by concentration separation in the wrinkled configuration. Such a step takes a much longer time than the first one because it involves long-range diffusion. Therefore, we can see that the evolution process of the diffusion-coupled wrinkle has a cascade feature, analogous to the discussion of the transformation sequences in the cubic → tetragonal decomposition [52–56]. There are two ranges of solvent concentration, within which the sequences of the formed wrinkling pattern are different. Figure 11 shows the evolution sequence of the wrinkling pattern and concentration profile in range A, where the computing parameters are taken as $\varepsilon_0 = 0.015$, $\varepsilon_c = 0.0077$, $\varepsilon_0' = 0$, $c_{\text{cri}} = 0.51$, and $c = 0.4$. The evolution involves two stages. In the first one, diffusion-driven concentration separation occurs but the film remains flat. The second stage starts when a concentration-rich domain attains a critical size through growth and coarsening. A domain of sufficiently large size undergoes a confined wrinkling transition as $c > c_{\text{cri}}' = \varepsilon_c'/\varepsilon_0$. ε_c' is a size-dependent critical wrinkling strain with $\varepsilon_c' > \varepsilon_c$ and $c > c_{\text{cri}}' > c_{\text{cri}} = 0.51$ (see the related result in Fig. 3). This is confirmed by the simulation result in Fig. 11, where the localized wrinkling occurs when the size of the concentration-rich domain is above a critical value. Another evolution sequence of the wrinkling pattern and concentration profile in range B with $c > c_{\text{cri}}$ is shown in

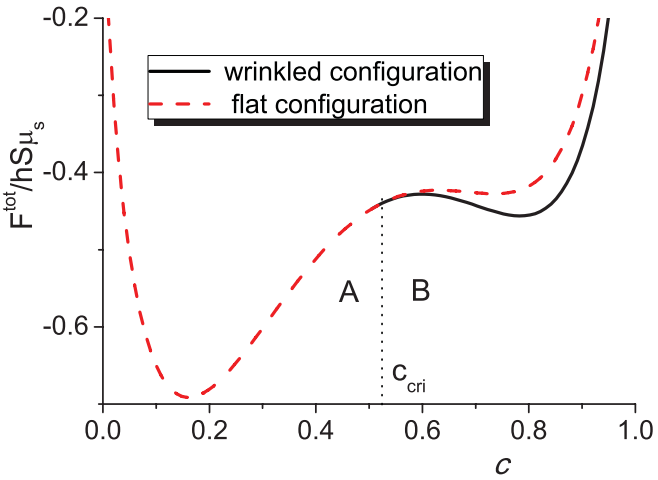

FIG. 10. (Color online) Typical total energy curves as a function of solvent concentration for the flat and sinusoidally wrinkled configuration in the film-substrate system.

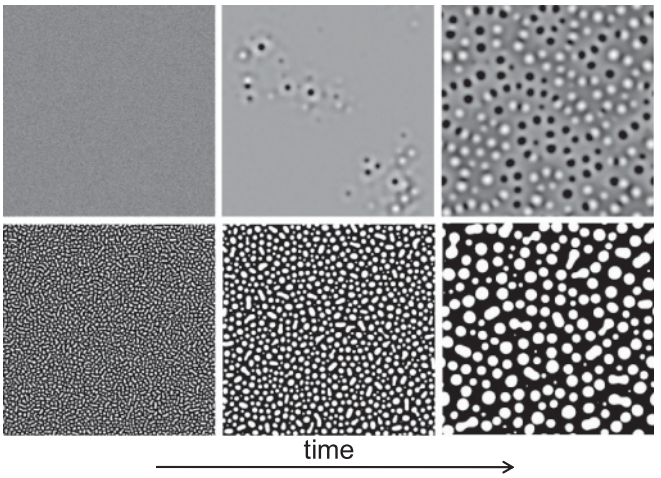

FIG. 11. Evolution sequence of the wrinkling pattern (top row) and concentration profile (bottom row) in mode A under the parameters $c = 0.4$, $\varepsilon_0 = 0.015$, and $\varepsilon_0' = 0$.

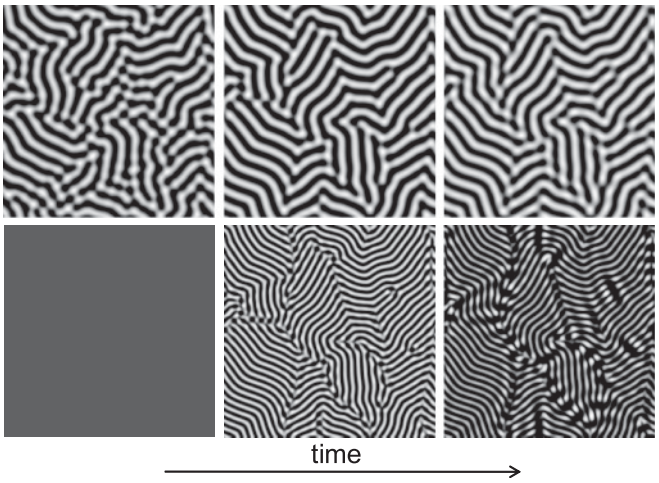

FIG. 12. Evolution sequence of the wrinkling pattern (top row) and concentration profile (bottom row) in mode B with the parameters $c = 0.4$, $\varepsilon_0 = 0.05$, and $\varepsilon_0' = 0$.

Fig. 12, where $\varepsilon_0 = 0.05$, $\varepsilon_0' = 0$, $c_{\rm cri} = 0.154$, and $c = 0.4$ are taken. The system first evolves into a labyrinth wrinkle without a concentration change. The wrinkle significantly influences the subsequent concentration separation, resulting in a concentration profile commensurate with the wrinkling morphology.

IV. DISCUSSIONS AND CONCLUSIONS

In the current model, the coupling between solvent diffusion and wrinkling originates from heterogeneous actuation strain caused by solvent diffusion, similar to the case of thermal expansion. Driven by an osmotic pressure, the solvent absorption may be inhomogeneous along both the direction of the film thickness and its lateral direction. The overall effect of any variation of the actuation strain induced by solvent absorption through the direction of the film thickness can be always specified as eigenstrain $\varepsilon^T_{\alpha\beta}$ and eigencurvature $k^T_{\alpha\beta}$ on the middle plane [50]:

$$\varepsilon^T_{\alpha\beta} = \frac{1}{h}\int_{-h/2}^{h/2} \varepsilon^*_{\alpha\beta}(\mathbf{x})dx_3,$$
$$k^T_{\alpha\beta} = \frac{12}{h^3}\int_{-h/2}^{h/2} x_3\varepsilon^*_{\alpha\beta}(\mathbf{x})dx_3, \tag{38}$$

If the inhomogeneity of the solvent concentration along the direction of the film thickness is small or symmetrically distributed across the middle plane, $k^T_{\alpha\beta} = 0$. Otherwise, there is a nonzero $k^T_{\alpha\beta}$. For a film with gradient elastic moduli on soft substrates, i.e., a confined hydrogel layer with gradient cross-linking density, the solvent concentration along the direction of the film thickness increases with the decrease of the shear modulus in the film since the distribution of the solvent through the thickness is roughly determined by the balance between the osmotic pressure and the compressive stress by solvent swelling in the film. Thus a positive (negative) stiffness gradient along the x_3 direction induces a negative (positive) $k^T_{\alpha\beta}$. In the experiment of Ref. [23], the solvent absorption in the film with increasing stiffness from the bottom to the top of the film corresponds to producing a negative $k^T_{\alpha\beta}$, while in the experiments of Refs. [25] and [26], solvent diffusion occurs in the film with increasing stiffness from the top to the bottom of the film, and there is a positive $k^T_{\alpha\beta}$. As we have shown in Figs. 6 and 8, positive $k^T_{\alpha\beta}$ facilitates formation of the hexagonal island array and negative $k^T_{\alpha\beta}$ favors the hexagonal dimple structure. The simulated results are consistent with experimental observations [23,25,26]. Although it seems that the assumption made in Eq. (1) could capture the main feature—that solvent diffusion creates spatiotemporal actuation strain and results in confined wrinkling instability comparable to experimental observations—the real situation between the swelling actuation strain and solvent concentration is much more complicated, and further quantitative study requires a nonlinear theory of coupled diffusion and finite swelling deformation in the film-substrate system, similar to the theory of polymeric gels [57,58].

In summary, nonlinear wrinkling of a thin film on a soft elastic substrate with diffusive solvent is explored through numerical simulation based on a continuum model. The results indicate that the solvent diffusion affects the wrinkling process in the following ways: (1) The diffusion-controlled actuation strain can regulate the distribution of the membrane stress, leading to size- and shape-dependent wrinkles. (2) The interplay between diffusion and wrinkle processes gives rise to spatiotemporal frustrations, where a rich variety of wrinkling patterns with nonuniform concentration, such as hexagonal order and peanut-shaped structures, can be formed, especially when the diffusion-controlled compression is slightly above the critical buckling strain. (3) The diffusion-controlled wrinkling process has a cascade feature. We hope that our study may be useful for engineering optimal surface wrinkles through the manipulation of the diffusion process.

ACKNOWLEDGMENTS

Y.N. is grateful to Jizhou Song for many helpful discussions. The authors gratefully appreciate financial support from the "Hundred of Talents Project" of the Chinese Academy of Sciences, the Chinese Natural Science Foundation (Grant Nos. 11072232 and 11072231) and the Basic Research Program of China (Grant Nos. 2011CB302100 and 2010CB934700).

[1] T. Tanaka, S. T. Sun, Y. Hirokawa, S. Katayama, J. Kucera, Y. Hirose, and T. Amiya, Nature (London) **325**, 796 (1987).
[2] H. Tanaka, H. Tomita, A. Takasu, T. Hayashi, and T. Nishi, Phys. Rev. Lett. **68**, 2794 (1992).
[3] N. Bowden, S. Brittain, A. G. Evans, J. W. Hutchingson, G. M. Witesides, and A. G. Evans, Nature (London) **393**, 146 (1998).
[4] W. T. S. Huck, N. Bowden, P. Onck, T. Pardoen, J. W. Hutchinson, and G. M. Whitesides, Langmuir **16**, 3497 (2000).

[5] P. J. Yoo, K. Y. Suh, S. Y. Park, and H. H. Lee, Adv. Mater. **14**, 1383 (2002).
[6] C. J. Rand, R. Sweeney, M. Morrissey, L. Hazel, and A. J. Crosby, Soft Matter **4**, 1805 (2008).
[7] J. Huang, M. Juszkiewicz, W. H. de Jeu, E. Cerda, T. Emrick, N. Menon, and T. P. Russell, Science **317**, 650 (2007).
[8] T. Ohzono and M. Shimomura, Phys. Rev. B **69**, 132202 (2004).
[9] E. P. Chan and A. J. Crosby, Soft Matter **2**, 324 (2006).
[10] S. K. Basu, A. V. McCormick, and L. E. Scriven, Langmuir **22**, 5916 (2006).
[11] P. C. Lin and S. Yang, Appl. Phys. Lett. **90**, 241903 (2007).
[12] A. Schweikart and A. Fery, Microchim. Acta **165**, 249 (2009).
[13] C. M. Stafford, C. Harrison, K. L. Beers, A. Karim, E. J. Amis, M. R. Vanlandingham, H. C. Kim, W. Volksen, R. D. Miller, and E. E. Simonyi, Nat. Mater. **3**, 545 (2004).
[14] K. Efimenko, M. Rackaitis, E. Manias, A. Vaziri, L. Mahadevan, and J. Genzer, Nat. Mater. **4**, 293 (2005).
[15] J. Genzer and J. Groenewold, Soft Matter **2**, 310 (2006).
[16] X. Chen and J. Yin, Soft Matter **6**, 5667 (2010).
[17] E. P. Chan, E. J. Smith, R. C. Hayward, and A. J. Crosby, Adv. Mater. **20**, 711 (2008).
[18] P. Lin, S. Vajpayee, A. Jagota, C. H. Hui, and S. Yang, Soft Matter **4**, 1830 (2008).
[19] E. P. Chan and A. J. Crosby, Adv. Mater. **18**, 3238 (2006).
[20] J. Yin, E. Bar-Kochba, and X. Chen, Soft Matter **5**, 3469 (2009).
[21] D. Y. Khang, H. Q. Jiang, Y. Huang, and J. A. Rogers, Science **311**, 208 (2006).
[22] H. Vandeparre and P. Damman, Phys. Rev. Lett. **101**,124301 (2008).
[23] D. Breid and A. J. Crosby, Soft Matter **5**, 425 (2009).
[24] J. Y. Chung, A. J. Nolte, and C. M. Stafford, Adv. Mater. **21**, 1358 (2009).
[25] M. Guvendiren, S. Yang, and J. A. Burdick, Adv. Funct. Mater. **19**, 3038 (2009).
[26] M. Guvendiren, J. A. Burdick, and S. Yang, Soft Matter **6**, 2044 (2010).
[27] H. Vandeparre, S. Gabriele, F. Brau, C. Gay, and K. K. Parker, Soft Matter **6**, 5751 (2010).
[28] D. C. Hyun, G. D. Moon, C. J. Park, B. S. Kim, Y. Xia, and U. Jeong, Adv. Mater. **22**, 1 (2010).
[29] H. G. Allen, *Analysis and Design of Structural Sandwich Panels* (Pergamon, New York, 1969).
[30] J. Groenewold, Physica A **298**, 32 (2001).
[31] E. Cerda and L. Mahadevan, Phys. Rev. Lett. **90**, 074302 (2003).
[32] J. Song, H. Jiang, W. M. Choi, D. Y. Khang, Y. Huang, and J. A. Rogers, J. Appl. Phys. **103**, 014303 (2008).
[33] B. Audoly and A. Boudaoud, J. Mech. Phys. Solids **56**, 2401 (2009).
[34] J. Song, H. Jiang, Y. Huang, and J. A. Rogers, J. Vac. Sci. Technol. A **27**,1107 (2009).
[35] J. Song, Appl. Phys. Lett. **96**, 051913 (2010).
[36] S. H. Im and R. Huang, J. Mech. Phys. Solids **56**, 3315 (2008).
[37] H. Q. Jiang, D. Y. Khang, J. Z. Song, Y. G. Sun, Y. G. Huang, and J. A. Rogers, Proc. Natl. Acad. Sci. USA **104**, 15607 (2007).
[38] N. Sridhar, D. J. Srolovitz, and Z. Suo, Appl. Phys. Lett. **78**, 2482 (2001).
[39] R. Huang and Z. Suo, J. Appl. Phys. **91**, 1135 (2002).
[40] Z. Y. Huang, W. Hong, and Z. Suo, Phys. Rev. E **70**, 030601 (2004).
[41] P. Peyla, Eur. Phys. J. B **48**, 379 (2005).
[42] R. Huang, J. Mech. Phys. Solids **53**, 63 (2005).
[43] R. Huang and S. H. Im, Phys. Rev. E **74**, 026214 (2006).
[44] N. Uchida and T. Ohzono, Soft Matter **6**, 5729 (2010).
[45] X. Chen and J. W. Hutchinson, J. Appl. Mech. **71**, 597 (2004).
[46] G. Cao, X. Chen, C. Li, A. Ji, and Z. Cao, Phys. Rev. Lett. **100**, 036102 (2008).
[47] J. Yin, Z. Cao, C. Li, I. Sheinman, and X. Chen, Proc. Natl. Acad. Sci. USA **105**, 19132 (2008).
[48] Z. Y. Huang, W. Hong, and Z. Suo, J. Mech. Phys. Solids **53**, 2101 (2005).
[49] A. G. Khachaturyan, *Theory of Structural Transformations in Solids* (Wiley, New York, 1983).
[50] E. H. Mansfield, *The Bending and Stretching of Plates*, 2nd ed. (Cambridge University Press, Cambridge, UK, 1989).
[51] L. Q. Chen and J. Shen, Comput. Phys. Commun. **108**, 147 (1998).
[52] A. G. Khachaturyan, T. F. Lindsey, and J. W. Morris, Metall. Mater. Trans. A **19**, 249 (1988).
[53] W. A. Soffa and D. E. Laughlin, Acta Metall. **37**, 3019 (1989).
[54] D. Fan and L. Q. Chen, J. Am. Ceram. Soc. **78**, 1680 (1995).
[55] Y. Ni, Y. M. Jin, and A. G. Khachaturyan, Acta Mater. **55**, 4903 (2007).
[56] Y. Ni and A. G. Khachaturyan, Nat. Mater. **8**, 410 (2009).
[57] W. Hong, X. H. Zhao, J. X. Zhou, and Z. Suo, J. Mech. Phys. Solids **56**,1779 (2008).
[58] M. K. Kang and R. Huang, J. Mech. Phys. Solids **58**, 1582 (2010).